J|A|C|S
JOURNAL OF THE AMERICAN CHEMICAL SOCIETY

Article

Cite This: *J. Am. Chem. Soc.* 2019, 141, 1280−1289

pubs.acs.org/JACS

A Dynamic Tetracationic Macrocycle Exhibiting Photoswitchable Molecular Encapsulation

Huang Wu,[‡,†] Yong Chen,[‡] Long Zhang,[†] Ommid Anamimoghadam,[†] Dengke Shen,[†] Zhichang Liu,[⊥] Kang Cai,[†] Cristian Pezzato,[†] Charlotte L. Stern,[†] Yu Liu,*[,‡,§] and J. Fraser Stoddart*[,†,∇,∥]

[‡]College of Chemistry, State Key Laboratory of Elemento-Organic Chemistry, Nankai University, 94 Weijin Road, Nankai District, Tianjin 300071, P. R. China

[†]Department of Chemistry, Northwestern University, 2145 Sheridan Road, Evanston, Illinois 60208, United States

[⊥]School of Science, Westlake University, 18 Shilongshan Road, Hangzhou 310024, China

[§]Collaborative Innovation Center of Chemical Science and Engineering (Tianjin), 92 Weijin Road, Nankai District, Tianjin 300072, P. R. China

[∇]School of Chemistry, University of New South Wales, Sydney, NSW 2052, Australia

[∥]Institute for Molecular Design and Synthesis, Tianjin University, 92 Weijin Road, Nankai District, Tianjin 300072, P. R. China

Supporting Information

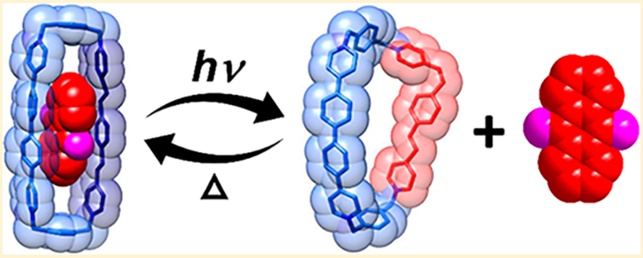

ABSTRACT: Designing macrocycles with appropriate molecular recognition features that allow for the integration of suitable external stimuli to control host−guest processes is a challenging endeavor which enables molecular containers to solubilize, stabilize, and separate chemical entities in an externally controllable manner. Herein, we introduce photo- and thermal-responsive elements into a semi-rigid tetracationic cyclophane, **OPVEx^{2}Box^{4+}**, that is composed of oligo(*p*-phenylenevinylene) pyridinium units and the biphenylene-bridged 4,4-bipyridinium extended viologens and adopts a rectangle-like geometry. It transpires that when the photoactive oligo(*p*-phenylenevinylene) pyridinium unit is incorporated in a macrocyclic scaffold, its reversibility is dramatically improved, and the configurations of the cyclophane can go back and forth between (*EE*)- and (*EZ*)-isomers upon alternating blue light irradiation and heating. When the macrocycle is found in its (*EE*)-configuration, it is capable of binding various π-electron-rich guests—e.g., anthracene and perylene—as well as π-electron-deficient guests—e.g., 9,10-anthraquinone and 5,12-tetracenequinone—through charge-transfer and van der Waals interactions. When irradiated with blue light, the (*EE*)-isomer of the cyclophane can be transformed successfully to the (*EZ*)-isomer, resulting in the switching off of the binding affinity for guest molecules, which are bound once again upon heating. The use of light and heat as external stimuli to control host−guest interactions involving a multi-responsive host and various guests provides us with a new opportunity to design and construct more-advanced molecular switches and machines.

INTRODUCTION

Allostery, triggered by external stimuli, enables tight regulation of protein functions in the cell environment.[1] Classical stereochemical models among the proteins are the tetrameric hemoglobins, which can go back and forth between relaxed and tense states upon catching or releasing oxygen.[2] In order to mimic nature's complex allosteric processes, the design and synthesis of well-crafted artificial macrocycles have long been a worthwhile goal[3] in supramolecular chemistry. Some of the intensively studied macrocyclic compounds, such as crown ethers,[4] cyclodextrins,[5] calixarenes,[6] and pillararenes,[7] possess various conformations featuring an optimal fit for the binding of diverse guest molecules. Positive allosterism,[8] however, permits turning on/off the behavior of macrocyclic hosts by external stimuli—for example, a reversible switch from predominantly bound to unbound or active to inactive structures[9]—which is important for developing new switchable catalysts[10] and sensors[11] and also possesses potential applications in separation and purification technologies.[12] A further series of dynamic molecular macrocycles,[13] cages,[14] and tweezers[15] have been developed that respond to pH,[13b] temperature,[13d] redox,[14a] interfacial tension,[15b] light,[16] and several other kinds of external stimuli. Among these external stimuli, light is the ideal candidate, owing to its non-invasive, clean, and remote-controllable nature, as well as the fact that it is easy to operate.[17] On the other hand, the concept of photocontrolled molecular encapsulation[18] is generally based on light-responsive guest molecules and, less frequently, host macrocycles, because the latter often suffer from tedious synthesis and also the tendency to hinder the isomerization of light-active species by ring strain or molecular crowding.[19]

Received: September 29, 2018
Published: November 26, 2018

DOI: 10.1021/jacs.8b10526
J. Am. Chem. Soc. 2019, 141, 1280−1289

Scheme 1. Synthesis of (*EE*)-MeOPV·2PF_6 and (*EE*)-OPVEx^{2}Box·4PF_6

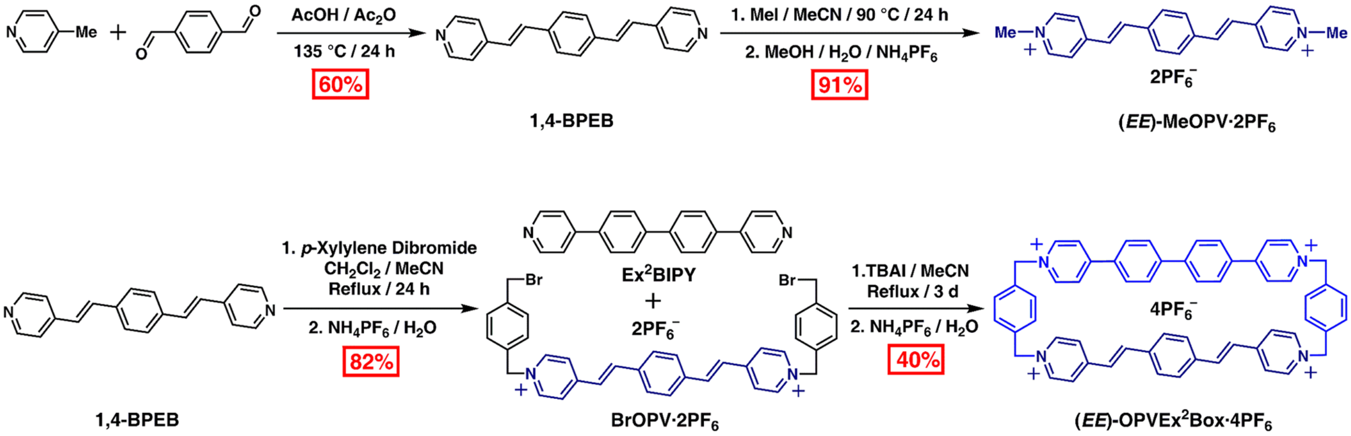

Photoactive host molecules, however, have much wider scope for applications than guest molecules. It is necessary, therefore, to identify eligible systems to break the logjam.[13a]

In addition, the rigid tetracationic cyclophane, cyclobis(paraquat-*p*-phenylene)[20] (**CBPQT^{4+}**), consisting of two π-electron-deficient bipyridinium units linked by *p*-xylylene bridges, has attracted a lot of attention, not only because of the well-defined inner cavity suitable for the encapsulation of π-electron-rich substrates—e.g., 1,5-dioxynaphthalene units[21] and tetrathiafulvalene derivatives[22]—but also because it serves as a vital building block for constructing mechanically interlocked molecules[23] (MIMs). In order to modulate the size of the cavity in **CBPQT^{4+}**, a series of "horizontal" *p*-phenylene connectors have been installed between the bipyridinium units. For example, **ExBox^{4+}** comprises two π-electron-poor 1,4-phenylene-bridged extended bipyridinium units, which endow it with the ability to bind a series of neutral polycyclic aromatic hydrocarbons (PAHs) of different sizes and shapes through donor−acceptor interactions.[12a] Then, **Ex^{2}Box^{4+}**, containing two biphenylene-bridged bipyridinium units, is capable of forming one-to-one complexes with polyether macrocycles—e.g., 1,5-dinaphtho[38]crown-10—or binding various long oligoacenes[24]—e.g., tetracene, tetraphene, and chrysene. By taking advantage of these outstanding host−guest properties and the semi-rigid structures of this extended-box family, we have incorporated photoactive elements into the semi-rigid organic cyclophane, (*EE*)-**OPVEx^{2}Box^{4+}**, which adopts (Scheme 1) a rectangle-like geometry and is composed of the photoactive oligo(*p*-phenylenevinylene) bipyridinium (OPV^{2+}) unit and the biphenylene-bridged 4,4-bipyridinium extended viologen (Ex^{2}BIPY^{2+}), connected end-to-end by *p*-xylylene linkers. The reversibility of the photo- and thermal-responsive OPV^{2+} unit is improved dramatically when it is incorporated into a macrocyclic scaffold, benefiting as it does from the ring strain in its (*EZ*)-configuration following blue light irradiation. The (*EE*)- and (*EZ*)-configurations of **OPVEx^{2}Box^{4+}** can be regulated reversibly by alternating blue light irradiation and heating, as confirmed by NMR, UV−vis absorption, and fluorescence spectroscopy and also by single-crystal X-ray diffraction (XRD). Moreover, on account of the distinct electronic character of (*EE*)-**OPVEx^{2}Box^{4+}**, it is capable of binding π-electron-rich—e.g., anthracene and perylene—as well as π-electron-deficient—e.g., 9,10-anthraquinone (**9,10-AQ**) and 5,12-tetracenequinone (**5,12-TQ**)—guest molecules through charge-transfer (CT) and van der Waals interactions. Most importantly of all, the corresponding guest molecules of diverse sizes, shapes, and electronic compositions can be taken up and released reversibly from the cavity of the **OPVEx^{2}Box^{4+}** by alternating irradiation with blue light and heating, as indicated by ^{1}H NMR and UV−vis absorption spectroscopies.

■ RESULTS AND DISCUSSION

The synthesis of (*EE*)-**OPVEx^{2}Box^{4+}** is shown in Scheme 1. Briefly, the Knoevenagel condensation between terephthalaldehyde and 4-picoline in acetic anhydride was carried out under reflux for 24 h to obtain **1,4-BPEB** in 60% yield. Subsequently, an S_N2 reaction between an excess of *p*-xylylene dibromide and **1,4-BPEB** in MeCN under reflux for 24 h led to the formation of **BrOPV**·2PF_6 after counterion exchange in a yield of 82%. Finally, equimolar amounts of **BrOPV**·2PF_6 and 4,4′-(4,4′-biphenylene)bipyridine (**Ex^{2}BIPY**) in the presence of tetrabutylammonium iodide (TBAI) in MeCN under reflux for 3 days in dark conditions, resulted in the isolation of the macrocycle (*EE*)-**OPVEx^{2}Box**·4Cl after workup by precipitation of the crude product with tetrabutylammonium chloride (TBACl). The desired product (*EE*)-**OPVEx^{2}Box**·4PF_6 was obtained after purification by reverse-phase column chromatography, followed by counterion exchange (NH_4PF_6/H_2O) in 40% yield. The compound was characterized by ^{1}H NMR (Figure S10), ^{13}C NMR (Figure S11), 2D ^{1}H−^{1}H COSY NMR (Figure S16), and 2D ROESY NMR (Figure S17) spectroscopies and also by high-resolution mass spectrometry (HRMS) (Figure S38). As a result of the asymmetric constitution of the (*EE*)-**OPVEx^{2}Box^{4+}**, the methylene protons were split into two sets of peaks (H_e/H_h, δ = 5.69/5.61 ppm), which were assigned by the analysis of both the one- and two-dimensional NMR spectra. HRMS revealed the presence of the $[M - PF_6]^+$ and $[M - 2PF_6]^{2+}$ species (m/z = 1235.2813 and 545.1585, respectively), which are consistent with the theoretical calculations.

The solid-state (super)structure of (*EE*)-**OPVEx^{2}Box**·4PF_6, which was determined by XRD analysis of a yellow single crystal obtained by slow vapor diffusion of Et_2O into a MeCN solution of (*EE*)-**OPVEx^{2}Box^{4+}** after 4 days, reveals an asymmetric, box-like geometry (Figure 1a), with average dimensions of 19.1 × 7.1 Å^2 (Figure 1b). The distances between the nitrogen atoms are 15.7 and 6.3 Å (Figure 1b,c), and the torsional angles of adjacent aromatic rings in the Ex^{2}BIPY^{2+} unit are ~26°, ~36°, and ~25°, respectively (Figure

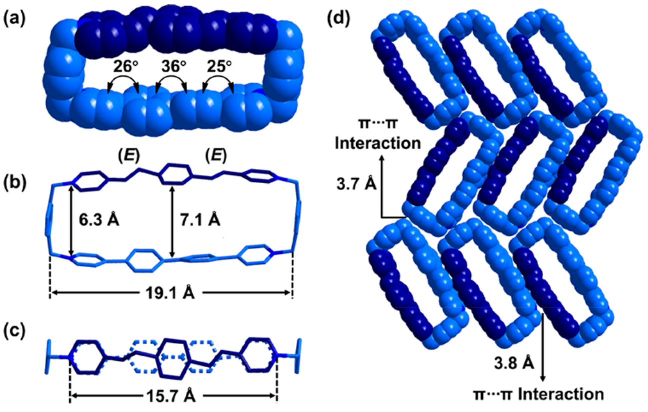

Figure 1. Solid-state (super)structure of (*EE*)-**OPVEx^{2}Box^{4+}** obtained from X-ray crystallography on single crystals of (*EE*)-**OPVEx^{2}Box**·4PF$_6$. (a) Space-filling representation showing the torsional angles of the Ex^{2}BIPY^{2+} unit (the torsional angles between adjacent aromatic rings are ~26°, ~36°, and ~25°, respectively) in (*EE*)-**OPVEx^{2}Box^{4+}**. (b,c) Stick representations of different side views showing the distances defining the box-like geometry. (d) Solid-state superstructure of (*EE*)-**OPVEx^{2}Box^{4+}** revealing a herringbone type of packing and two kinds of $\pi\cdots\pi$ interactions. The hydrogen atoms, counterions, and solvent molecules are omitted for the sake of clarity.

1a). The solid-state superstructure (Figure 1d) of (*EE*)-**OPVEx^{2}Box^{4+}** reveals that it crystallizes in the monoclinic space group $P2_1/c$ with the molecules packing in a herringbone fashion. There is only partial $\pi\cdots\pi$ stacking between the Ex^{2}BIPY^{2+} unit and the OPV^{2+} unit, with a distance of 3.8 Å between adjacent cyclophanes, and the residual pyridinium groups in both the Ex^{2}BIPY^{2+} and the OPV^{2+} units aptly stack with the *p*-xylylene rings in the closest adjacent cyclophanes via a $\pi\cdots\pi$ interaction with a distance of 3.7 Å, which may arise from the balance between Coulombic repulsions and the maximization of π-overlap in the entire superstructure.[25]

Because of the presence of the stilbene moiety, it was anticipated[26] that (*EE*)-**OPVEx^{2}Box^{4+}** might undergo (*E*)→(*Z*) isomerization upon light irradiation. The UV−vis absorption spectrum (Figures 3 and Figure S1) of (*EE*)-**OPVEx^{2}Box^{4+}** revealed an absorption peak up to 470 nm, suggesting it might undergo photoisomerization upon irradiation with blue light. The photoisomerization of (*EE*)-**OPVEx^{2}Box^{4+}** was first investigated by ^{1}H NMR spectroscopy. The ^{1}H NMR spectrum (Figures 2 and S20) of a freshly prepared CD$_3$CN solution of (*EE*)-**OPVEx^{2}Box^{4+}** showed two distinct sets of proton resonances upon blue light (450−460 nm) irradiation, indicative of (*EE*)-**OPVEx^{2}Box^{4+}** undergoing isomerization. The resonances of the protons H$_k$ and H$_l$

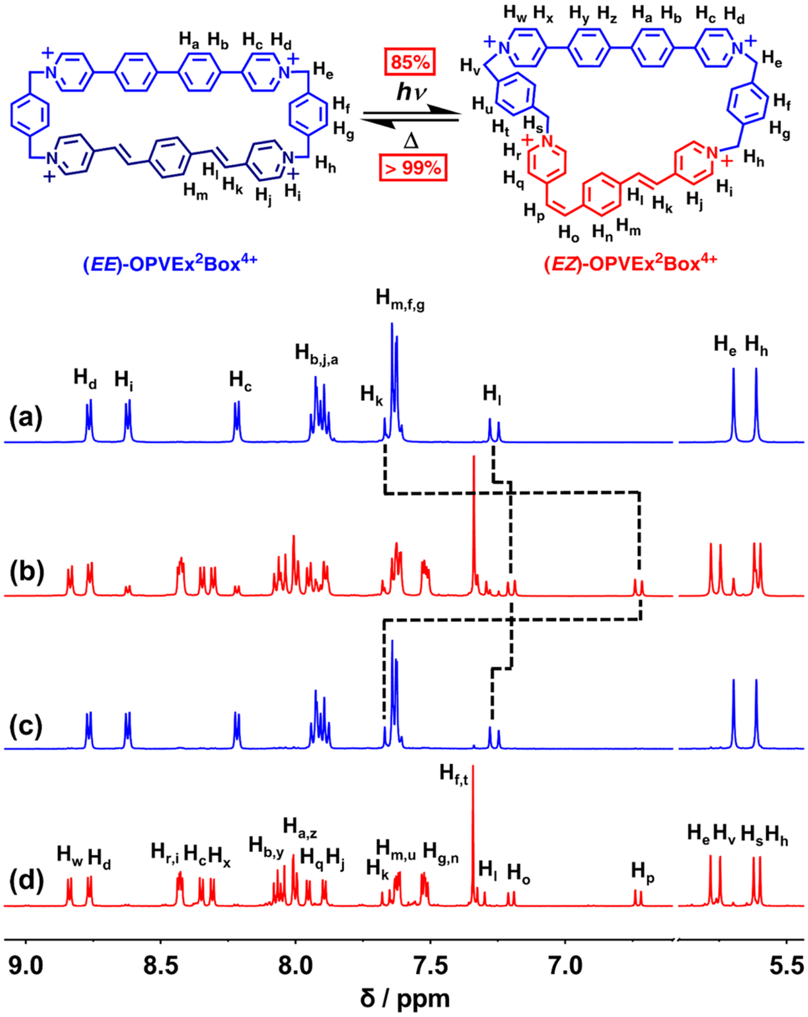

Figure 2. ^{1}H NMR spectra (500 MHz, CD$_3$CN, 298 K) of (*EE*)-**OPVEx^{2}Box**·4PF$_6$ (a) before and (b) after blue light irradiation (450−460 nm, 12 W, 12 s). (c) Spectrum after heating the solution of (b) for 16 h at 70 °C. (d) Spectrum of (*EZ*)-**OPVEx^{2}Box**·4PF$_6$.

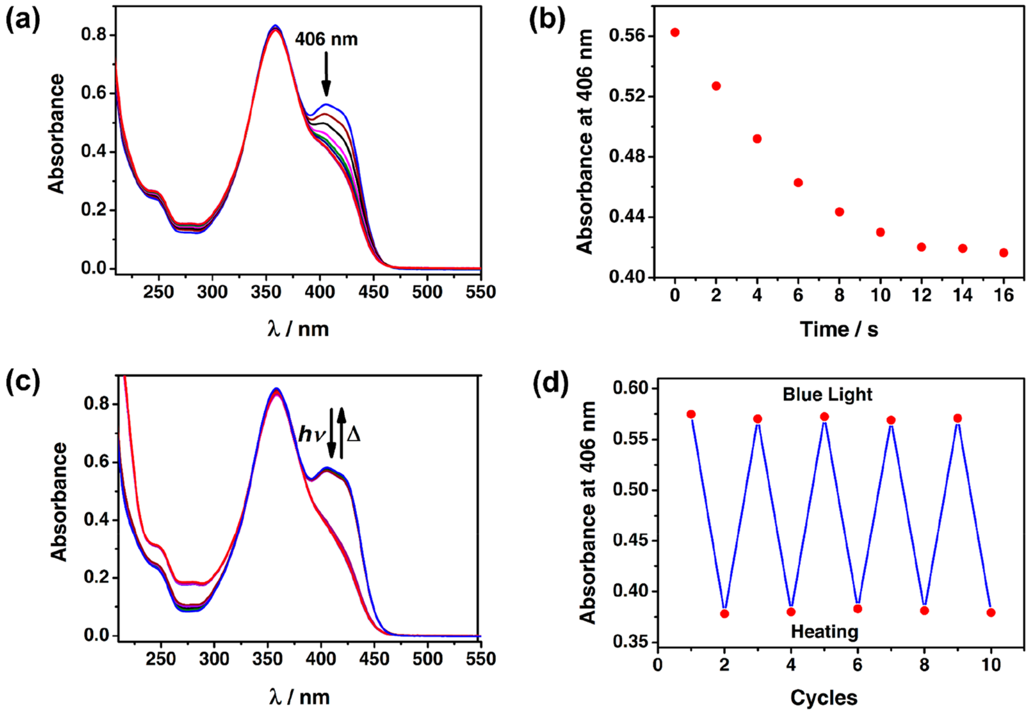

Figure 3. (a) UV−vis absorption spectra (10 μM in MeCN, 298 K) and (b) absorbance intensity changes at 406 nm of **OPVEx^{2}Box^{4+}** upon irradiation with blue light (450−460 nm, 1 W, 16 s). (c) UV−vis absorption spectra (10 μM in MeCN, 298 K) and (d) absorbance intensity changes at 406 nm of **OPVEx^{2}Box^{4+}** upon alternating blue light irradiation (450−460 nm, 1 W, 12 s) and heating (70 °C, 10 min).

residing on the C═C double bond were split into two sets: the original set was assigned to the unreacted species, while the other set of proton resonances (Figure 2b), H_o (d, J = 12.9 Hz) and H_p (d, J = 12.8 Hz), was attributed to the transformation of **OPVEx^{2}Box^{4+}** from the (*EE*)- to the (*EZ*)-isomer. The intensity of the proton signals (Figure S20) of (*EE*)-**OPVEx^{2}Box^{4+}** gradually decreased, accompanied by the increase of the (*EZ*)-**OPVEx^{2}Box^{4+}** proton resonances, with prolonged irradiation. According to the relative integrals of the protons, the ratio of the (*EE*)- and the (*EZ*)-isomers was calculated to be 15:85 in the photostationary state (PSS). The non-quantitative conversion from the (*EE*)- to the (*EZ*)-isomers under irradiation with blue light is probably a result of overlapping of the absorbance spectra of the (*EE*)- and the (*EZ*)-isomers (Figure S1). In order to confirm the isomerization of the OPV^{2+} unit, a reference compound, (*EE*)-**MeOPV^{2+}**, was synthesized (Scheme 1) and characterized by ^{1}H NMR (Figure S8), ^{13}C NMR (Figure 9), 2D ^{1}H−^{1}H COSY NMR (Figure S14), and 2D NOESY NMR (Figure S15) spectroscopies and also by HRMS (Figure S36). ^{1}H NMR spectroscopic changes in the chemical shifts of the protons residing on the C═C double bond associated with the (*EE*)→(*EZ*) isomerization in **MeOPV^{2+}** (Figure S23) are similar to those observed in the case of **OPVEx^{2}Box^{4+}**. Upon irradiation of the MeCN solution of (*EE*)-**MeOPV^{2+}** for 10 s, the conversion yield (Figure S23) from the (*EE*)- to the (*EZ*)-isomers is 90%, which is a little higher than the 85% yield obtained for (*EE*)-**OPVEx^{2}Box^{4+}**. The (*ZZ*)-isomer was not detected in the light-promoted isomerization of both **OPVEx^{2}Box^{4+}** and **MeOPV^{2+}**, a situation which can possibly be ascribed to the (*EZ*)-isomers following irradiation showing (Figure 3a and S1) very weak absorption for the blue light (450−460 nm). On heating of the solution of the PSS (*EZ*)-**OPVEx^{2}Box^{4+}** at 70 °C for 16 h, the ^{1}H NMR spectra (Figure 2c and S21) indicated almost quantitative conversion of the (*EZ*)-isomer into the (*EE*)-isomer. Moreover, this interconversion can be repeated through several cycles without any appreciable light fatigue being evident (Figure S22) upon alternating blue light irradiation and heating. In the case of **MeOPV^{2+}**, however, the (*EZ*)-isomer could not be transformed completely (Figure S24) into the (*EE*)-isomer, even after heating at 70 °C for up to 144 h. The ratio of the (*EE*)- to the (*EZ*)-isomers was calculated to be 75:25 in the thermal steady state. Comparing **OPVEx^{2}Box^{4+}** with **MeOPV^{2+}**, it can be concluded that the ring effect improves significantly the conversion yield and the reaction rate of the reverse (*EZ*)→(*EE*) isomerization upon heating.

The isomerizations exhibited by **OPVEx^{2}Box^{4+}** and **MeOPV^{2+}** were also studied by UV−vis absorption and fluorescence spectroscopies. The UV−vis absorption spectrum (Figure 3a) of the (*EE*)-**OPVEx^{2}Box^{4+}** exhibits two strong absorption peaks at 359 and 406 nm, which can be assigned to the characteristic absorptions of the Ex^{2}BIPY^{2+} and OPV^{2+} units, respectively. After a MeCN solution of (*EE*)-**OPVEx^{2}Box^{4+}** had been irradiated with blue light (450−460 nm) for 12 s, the intensity of the band at 406 nm (Figure 3a,b), corresponding to the absorption of the OPV^{2+} unit, decreased gradually and was accompanied by a slight increase in the intensity of the absorption band at 220−350 nm. These changes can be directly ascribed to the transformation of **OPVEx^{2}Box^{4+}** from the (*EE*)- to (*EZ*)-isomers. When the solution of the PSS of (*EZ*)-**OPVEx^{2}Box^{4+}** was heated at 70 °C for 10 min, the UV−vis absorption spectrum (Figure 3c) all but recovered to that of the (*EE*)-isomer. On the other hand, with excitation at 359 nm, the fluorescence spectrum (Figure S5) of (*EE*)-**OPVEx^{2}Box^{4+}** revealed an emission at λ_{max} = 485 nm. The fluorescence intensity of **OPVEx^{2}Box^{4+}** was quenched gradually (Figure S6) upon irradiation with blue light (450−460 nm) for 12 s. The changes in the fluorescence spectrum also indicate the conversion of **OPVEx^{2}Box^{4+}** from the (*EE*)- to (*EZ*)-isomers upon irradiation with blue light. Moreover, this interconversion could be repeated through several cycles without any noticeable fatigue (Figure 3c,d), an observation which is consistent with that (Figure S22) from the ^{1}H NMR spectroscopy. These two experiments demonstrated jointly the prominent photo- and thermal-switched configurational interconversion properties of **OPVEx^{2}Box^{4+}**. The changes in the UV−vis absorption (Figure S2) and fluorescence (Figure S7) spectra associated with the photoisomerization of **MeOPV^{2+}** are analogous to those observed for **OPVEx^{2}Box^{4+}**. The absorption peak at 392 nm and the fluorescence peak at 474 nm decreased gradually upon irradiation with blue light (450−460 nm), as a result of the conversion from the (*EE*)- into the (*EZ*)-isomers. When the MeCN solution of the PSS (*EZ*)-**MeOPV^{2+}** was heated at 70 °C for 50 min, the absorption spectrum, however, did not revert (Figure S3a) to its original state, demonstrating that the (*EZ*)-isomer cannot be completely converted into the (*EE*)-isomer. In three cycles of alternating blue light irradiation and heating, the absorption peak at 392 nm became (Figure S3b) lower and lower and was accompanied by the appearance of a new peak at 274 nm, indicating that some photochemical side reactions were occurring during light irradiation.[27] Considering the photophysical properties and the isomerization of both **OPVEx^{2}Box^{4+}** and **MeOPV^{2+}**, it can be concluded that the photoisomerization of the OPV^{2+} unit from the (*EE*)- to the (*EZ*)-configuration was not barred within the macrocyclic scaffold. On the contrary, incorporation of the cyclophane improved drastically the reversibility of the OPV^{2+} unit, especially in the conversion yield and the reaction rate from the (*EZ*)- into the (*EE*)-isomers upon heating.

In an effort to investigate thoroughly the reason for the ring effect improving the reversibility of the OPV^{2+} unit, the (*EZ*)-**OPVEx^{2}Box^{4+}** was isolated (Scheme S6) by reverse-phase preparative HPLC after blue light irradiation. The ^{1}H NMR (Figure S12), ^{13}C NMR (Figure S13), and HRMS (Figure S39) of (*EZ*)-**OPVEx^{2}Box^{4+}** all indicated the existence of a single compound, in which the complete assignment of all the proton resonances was achieved by 2D ^{1}H−^{1}H COSY NMR (Figure S18) and 2D ROESY NMR (Figure S19) spectroscopies. Specific information on the configuration was obtained from the single-crystal XRD. X-ray structural analysis shows that the solid-state structure (Figure 4) of the (*EZ*)-**OPVEx^{2}Box^{4+}** is distinctly different from the rectangle-like structure adopted by (*EE*)-**OPVEx^{2}Box^{4+}**. The configuration of the OPV^{2+} unit changes from a linear to a "seven"-like geometry, as a result of the photoisomerization causing the (*EE*)-isomer to be converted into the (*EZ*)-isomer after blue light irradiation. The distance (Figure 4b) between the two nitrogens in the OPV^{2+} unit (N_3−N_4) is 12.9 Å, which is shorter than the distance (15.7 Å) in (*EE*)-**OPVEx^{2}Box^{4+}**. The isomerization of the OPV^{2+} unit affects the conformations adopted by every component in the cyclophane, because of the ring effect. The two *p*-xylylene units are tilted (Figure 4a) with respect to each other, with a dihedral angle of 86°, which is quite different from the almost parallel arrangement in (*EE*)-**OPVEx^{2}Box^{4+}**. The Ex^{2}BIPY^{2+} unit is compelled to bend into the cavity of the cyclophane, with a distance between the two nitrogens (N_1−N_2) of 15.1 Å (Figure 4b), which is also shorter than that (15.7 Å) in (*EE*)-**OPVEx^{2}Box^{4+}**. The strain arising from the curving Ex^{2}BIPY^{2+} unit may be the reason for the reversibility of the OPV^{2+} unit being improved when it is incorporated in the macrocycle, **OPVEx^{2}Box^{4+}**. The distance between N_1−N_3 and N_2−N_4 increases to 7.2 and 6.7 Å, respectively (Figure 4a), from the initial 6.3 Å in (*EE*)-**OPVEx^{2}Box^{4+}**. On the other hand, the Ex^{2}BIPY^{2+} and OPV^{2+} units in (*EZ*)-**OPVEx^{2}Box^{4+}** do not adopt a face-to-face arrangement (Figure 4b), which is different from the aspectant arrangement in (*EE*)-**OPVEx^{2}Box^{4+}**. The solid-state superstructure of (*EZ*)-**OPVEx^{2}Box^{4+}** reveals a layered stacking in which the molecules crystallize in the monoclinic space group *C*2/*c*. The adjacent (*EZ*)-**OPVEx^{2}Box^{4+}** adopts (Figure 4c) a face-to-face stacking geometry incorporating $\pi\cdots\pi$ interactions between the adjacent Ex^{2}BIPY^{2+} and (*EZ*)-OPV^{2+} units with a distance of 3.4 Å along the *c*-axis. The three-dimensional superstructure was achieved by the two-level assemblies—first in the adjacent layers through $\pi\cdots\pi$ interactions between two (*EZ*)-OPV^{2+} units with a distance of 3.6 Å to form a bilayer (Figure 4d), and then a further assembly sustained by electrostatic and hydrogen-bonding interactions.

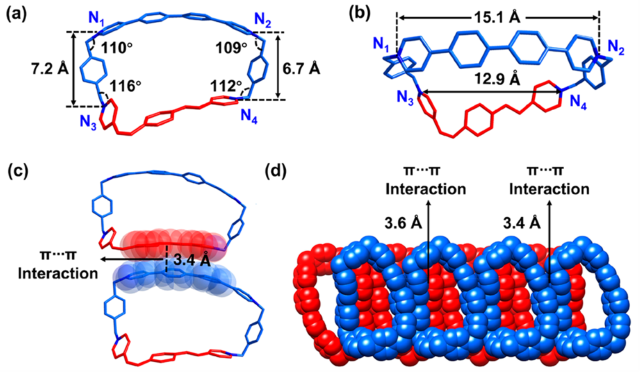

Figure 4. Solid-state (super)structure of (*EZ*)-**OPVEx^{2}Box^{4+}** obtained from X-ray crystallography on single crystals of (*EZ*)-**OPVEx^{2}Box**·4PF$_6$. (a,b) Stick representations of different side views of (*EZ*)-**OPVEx^{2}Box^{4+}**, showing the distances and angles associated with the geometry after blue light irradiation. (c) Solid-state superstructure showing the face-to-face stacking between the adjacent Ex^{2}BIPY^{2+} and (*EZ*)-OPV^{2+} units in adjacent (*EZ*)-**OPVEx^{2}Box^{4+}** molecules. (d) Space-filling representations of the (*EZ*)-**OPVEx^{2}Box^{4+}** superstructure revealing a bilayer type of packing involving two kinds of $\pi\cdots\pi$ interactions. The hydrogen atoms, counterions, and solvent molecules are omitted for the sake of clarity.

The constitution of **OPVEx^{2}Box^{4+}** is based on the family of well-known "extended viologen cyclophanes",[28] which possess high affinity for binding PAHs as a result of CT interactions between the π-electron-poor viologens and π-electron-rich aromatic rings. In the case of (*EE*)-**OPVEx^{2}Box^{4+}**, however, one bipyridium ring is bridged by a biphenylene subunit, while another is linked by a *p*-divinylbenzene subunit. These longer linkers may be responsible for the electronic distortions in the "extended viologen" units.[24] It is possible, therefore, for (*EE*)-**OPVEx^{2}Box^{4+}** to exploit multiple modes of binding different guests with various electronic configurations. In order to confirm the binding diversity of (*EE*)-**OPVEx^{2}Box^{4+}**, two π-electron-rich guests—e.g., anthracene and perylene—and two π-electron-deficient guests—e.g., **9,10-AQ** and **5,12-TQ**—were selected as representative examples. High-quality single crystals of their 1:1 complexes were obtained by slow vapor diffusion of *i*Pr$_2$O into a solution of (*EE*)-**OPVEx^{2}Box^{4+}** containing excesses of guest molecules in MeCN over a period of one week. The XRD analyses of these single crystals reveal

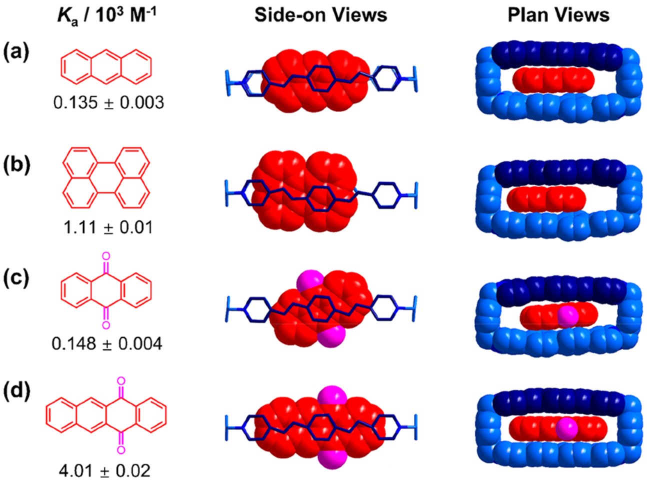

Figure 5. Structural formulas of the guests and the corresponding K_a values for binding inside (*EE*)-**OPVEx^{2}Box^{4+}** obtained by ^{1}H NMR titrations in CD_3CN (left), and side-on (middle) and plan (right) views of the stick/space-filling representations of the solid-state superstructures of the complexes of (*EE*)-**OPVEx^{2}Box^{4+}** with (a) anthracene, (b) perylene, (c) **9,10-AQ**, and (d) **5,12-TQ**. The hydrogen atoms, counterions, and solvent molecules are omitted for the sake of clarity.

(Figure 5) the various binding modes and diverse superstructures of the complexes.

In the case of the π-electron-rich guests, the colors of the crystals reflect directly the CT interaction between the host and guests, a situation which could also be indicated (Figure S4) by the corresponding CT bands in the absorption spectra. The crystals of the anthracene⊂(*EE*)-**OPVEx^{2}Box^{4+}** complex are deep yellow (Figure S4a, inset), while those of the perylene⊂(*EE*)-**OPVEx^{2}Box^{4+}** complex are orange (Figure S4b, inset), making it convenient to detect them visually when the electron-rich guests are complexed inside the cavity of the cyclophane. The long axis of the anthracene is (Figures 5a and S42) almost aligned along the one side of the cyclophane, and it is positioned closer to one end of the cyclophane than the other, a situation which can be achieved with the assistance of change-transfer interactions at the end of the cyclophane and favorable van der Waals interactions in the center. The binding mode of perylene inside the cavity of (*EE*)-**OPVEx^{2}Box^{4+}** is analogous to that of anthracene. The long axis of perylene almost adopts (Figures 5b and S43) a parallel arrangement inside the (*EE*)-**OPVEx^{2}Box^{4+}**. The host-guest complexes of anthracene and perylene show analogous stacking in the solid-state superstructure. A 2:1 ratio is observed between anthracene and (*EE*)-**OPVEx^{2}Box^{4+}** in the crystal, wherein one anthracene molecule is located inside the cavity of the cyclophane and the other is located outside (Figure S42). Similarly, perylene co-crystallizes with (*EE*)-**OPVEx^{2}Box^{4+}** in a ratio of 7:4, wherein one perylene molecule is positioned inside the cavity of the host and the remaining perylene molecules are accommodated (Figure S43) in the space between two host−guest complexes. In contrast, the binding mode between (*EE*)-**OPVEx^{2}Box^{4+}** and electron-deficient guests is different from that of the electron-rich guests. The **9,10-AQ** resides in the center of the cyclophane, accompanied (Figures 5c and S44) by a tilt angle of 24°, which is caused by the π-electron-poor central quinone substructure in **9,10-AQ** that is prone to overlap with the π-electron-rich biphenylene and divinylbenzene units in the center of (*EE*)-**OPVEx^{2}Box^{4+}**. On the other hand, **5,12-TQ** is (Figure 5d and S45) completely aligned along its long axis inside the center of the cavity, and the π-electron-poor quinone subunit is 1.3 Å distant from the central position of (*EE*)-**OPVEx^{2}Box^{4+}**, achieving maximized $\pi-\pi$ overlap between host and guest. Both the **9,10-AQ**⊂(*EE*)-**OPVEx^{2}Box^{4+}** and **5,12-TQ**⊂(*EE*)-**OPVEx^{2}Box^{4+}** are crystallized in 1:1 host−guest complexes instead of forming co-crystals between the complex and an excess of guests. In the case of the **9,10-AQ**⊂(*EE*)-**OPVEx^{2}Box^{4+}**, the complexes are integrated by $\pi\cdots\pi$ interaction between the Ex^{2}BIPY^{2+} and OPV^{2+} units to form (Figure S44) a layered superstructure, while the **5,12-TQ**⊂(*EE*)-**OPVEx^{2}Box^{4+}** relies on ion−dipole interactions between the positively charged pyridinium units in (*EE*)-**OPVEx^{2}Box^{4+}** and the carbonyl group in complexed **5,12-TQ** to form (Figure S45) a sandwich superstructure, revealing that changing the guest molecule is a feasible way to modulate crystal superstructures.

In order to elucidate the binding affinity of (*EE*)-**OPVEx^{2}Box^{4+}** toward guest molecules in solution, their complexes with (*EE*)-**OPVEx^{2}Box^{4+}** were investigated by ^{1}H NMR spectroscopy and HRMS. The ^{1}H NMR spectra (Figure 6) of the complexes formed by (*EE*)-**OPVEx^{2}Box^{4+}** with both the π-electron-rich guests—e.g., anthracene and perylene—and π-electron-poor guests—e.g., **9,10-AQ** and **5,12-TQ**—all show characteristic upfield shifts. The resonances corresponding to protons H_a, H_b on the biphenylene, H_k, H_l, H_m on the divinylbenzene, H_c, H_j on the pyridinium rings in (*EE*)-**OPVEx^{2}Box^{4+}**, and the protons in the guest molecules all show an obvious upfield shift. These results reveal that the guest molecules are included inside the cavity of the cyclophane. The specific changes in chemical shift for the individual protons of guest molecules were investigated in detail. The chemical shifts of the protons (H_α, H_β and H_γ) in anthracene underwent (Figure 6b) appreciable upfield shifts ($\Delta\delta$ = 0.07, 0.06, and 0.06 ppm for H_α, H_β, and H_γ, respectively). The proton signals of perylene displayed (Figure 6c) significant upfield shifts ($\Delta\delta$ = 0.15, 0.14, and 0.22 ppm for H_α, H_β, and H_γ, respectively). In addition, the π-electron-poor guests **9,10-AQ** and **5,12-TQ** were also investigated. The chemical shifts of the protons (H_α and H_β) in **9,10-AQ** exhibited (Figure 6d) appreciable upfield shifts ($\Delta\delta$ = 0.10 and 0.14 ppm for H_α and H_β, respectively). The resonances for each of the protons in **5,12-TQ**, however, displayed considerable upfield shifts (Figure 6e), in which the protons H_α and H_β exhibited the largest upfield shifts ($\Delta\delta$ = 1.10 and 1.06 ppm for H_α and H_β, respectively), while the other protons displayed upfield shifts in the range of 0.41−0.44 ppm, which can be attributed to additional shielding of protons H_α and H_β by the *p*-xylylene at the two ends of the cyclophane. The Job's plots for anthracene (Figure S26b), perylene (Figure S28b), **9,10-AQ** (Figure S30b), and **5,12-TQ** (Figure S32b) with (*EE*)-**OPVEx^{2}Box^{4+}** all show maxima at a molar fraction of 0.5, indicating a stoichiometric ratio of 1:1. The association constant between (*EE*)-**OPVEx^{2}Box^{4+}** and perylene (1.11×10^3 M^{-1}) (Figures S27 and S28a) is significantly larger than that (135 M^{-1}) observed for anthracene (Figures S25 and S26a), and the K_a value (4.01×10^3 M^{-1}) for the complexation of (*EE*)-**OPVEx^{2}Box^{4+}** with **5,12-TQ** (Figures S31 and S32a) is also larger than that (148 M^{-1}) with **9,10-AQ** (Figures S29 and S30a). These significant increases in the association constants suggest that the aromatic core of guest molecules has a significant influence on the association constant, with larger π-systems resulting in greater $\pi-\pi$ interactions between host and guests.[29] Moreover, the formation of 1:1 complexes was

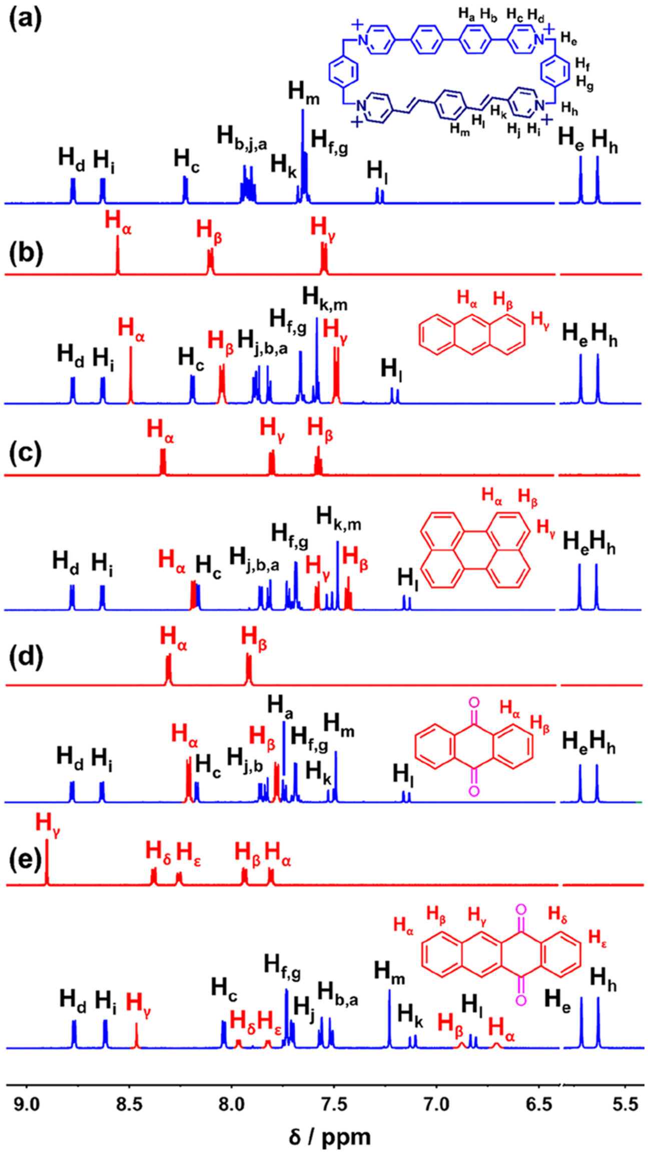

Figure 6. Partial ^{1}H NMR spectra (600 MHz, CD_3CN, 298 K) of (a) (*EE*)-**OPVEx^{2}Box^{4+}** and its complexes with (b) anthracene, (c) perylene, (d) **9,10-AQ**, and (e) **5,12-TQ**. The ^{1}H NMR spectra (red) of the unbound guests in CD_3CN are shown above the ^{1}H NMR spectra of the individual complexes (blue for the (*EE*)-**OPVEx^{2}Box^{4+}** and red for the bound-guest signals) in (b−e).

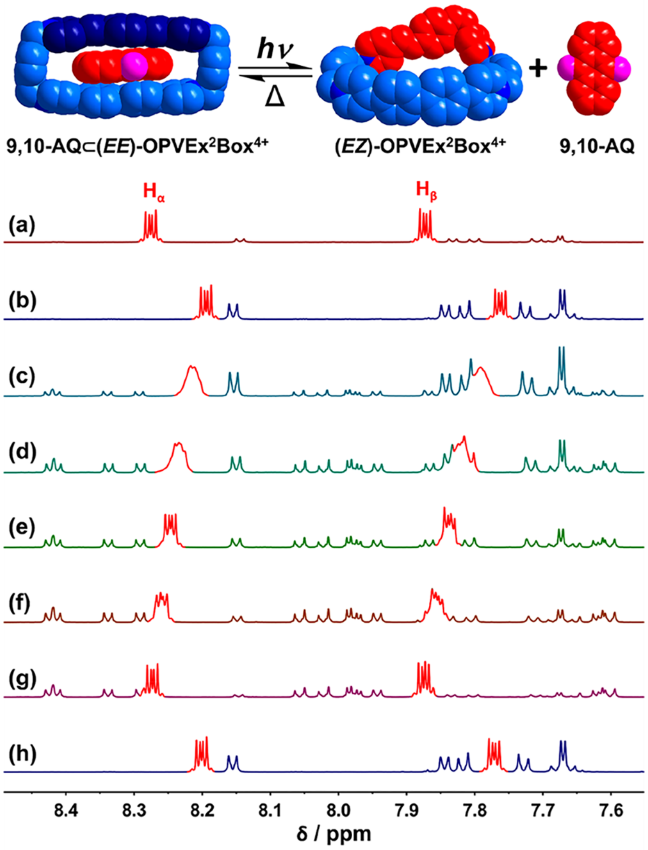

Figure 7. Partial ^{1}H NMR spectra (600 MHz, CD_3CN, 298 K) of (a) **9,10-AQ** with 15% (*EE*)-**OPVEx^{2}Box^{4+}**, and **9,10-AQ**⊂(*EE*)-**OPVEx^{2}Box^{4+}** complex (b) before and (c−g) after blue light (450−460 nm, 12 W) irradiation for (c) 2 s, (d) 4 s, (e) 6 s, (f) 8 s, and (g) 10 s. (h) Spectrum after heating the solution of (g) at 70 °C for 16 h. The resonance peaks for the protons in **9,10-AQ** are indicated in red color.

also confirmed by HRMS. The HRMS spectra of the anthracene⊂(*EE*)-**OPVEx^{2}Box^{4+}** (Figure S40) and perylene⊂(*EE*)-**OPVEx^{2}Box^{4+}** (Figure S41) show molecular ion peaks at 1413.36 and 1487.37, assigned to [anthracene⊂(*EE*)-**OPVEx^{2}Box**·4PF$_6$− PF$_6$]$^+$ and [perylene⊂(*EE*)-**OPVEx^{2}Box**·4PF$_6$ − PF$_6$]$^+$, respectively.

The remarkable photo- and thermal-induced isomerization and abundant host−guest interactions of **OPVEx^{2}Box^{4+}** led us to investigate the photo- and thermal-controlled uptake and release of guest molecules. Upon exposure of the **9,10-AQ**⊂(*EE*)-**OPVEx^{2}Box^{4+}** complex to blue light (450−460 nm), the (*EE*)→(*EZ*) isomerization of the host is initiated, and the signals of the **9,10-AQ** protons (H_α and H_β) in the host−guest complex undergo (Figure 7c−g) a downfield shift gradually upon irradiation with blue light, indicating that the **9,10-AQ** is expelled increasingly away from the cavity of **OPVEx^{2}Box^{4+}**. Upon irradiation of the complex with blue light (450−460 nm) for 10 s (Figure 7g), the chemical shifts of H_α and H_β were identical with those of the reference ^{1}H NMR spectrum (Figure 7a) containing 15% host, which shows that the (*EZ*)-**OPVEx^{2}Box^{4+}** has little or no binding affinity for **9,10-AQ**. When the PSS mixture was heated in CD_3CN solution at 70 °C for 16 h, the chemical shifts of protons in **9,10-AQ** recovered to their original values (Figure 7h), revealing that **9,10-AQ** is bound inside the cavity of (*EE*)-**OPVEx^{2}Box^{4+}** once again. The efficient release and uptake of *π*-electron-poor guests can also be confirmed by irradiating and heating a CD_3CN solution of the **5,12-TQ**⊂(*EE*)-**OPVEx^{2}Box^{4+}** complex. The signals of the **5,12-TQ** protons are shifted (Figure S33) downfield upon exposure to blue light and subsequently recover their initial values upon heating. In the case of the *π*-electron-rich guests, similar release and uptake processes were observed in the ^{1}H NMR spectra upon alternating blue light irradiation and heating. Upon irradiation of the CD_3CN solution of the anthracene⊂(*EE*)-**OPVEx^{2}Box^{4+}** complex with blue light (450−460 nm), the signals for anthracene protons undergo (Figure S34) a downfield shift, where most of anthracene is released during 12 s (Figure S34h), revealing that the light-controlled guest release process is also functioning with *π*-electron-rich guests. On heating of the CD_3CN solution of the anthracene⊂(*EE*)-**OPVEx^{2}Box^{4+}** complex after irradiation, the chemical shifts of the anthracene

DOI: 10.1021/jacs.8b10526
J. Am. Chem. Soc. 2019, 141, 1280−1289

protons return (Figure S34i) to the initial values. In order to confirm the photo-controlled π-electron-rich guest-encapsulated process, the perylene⊂(*EE*)-**OPVEx^{2}Box^{4+}** complex was also investigated by ^{1}H NMR spectroscopy. Downfield shifts were observed (Figure S35) for the signals of perylene protons upon blue light irradiation and the chemical shifts of the protons in perylene returned to their original values after heating. The photo-controlled release process of π-electron-rich guests was also demonstrated (Figure S4) by UV−vis absorption spectroscopy. The CT bands between host−guest complexes and the host or guests decrease dramatically after blue light irradiation, owing to the isomerization of the OPV^{2+} unit, leading to the release of the guest molecules. All of these results prove that the isomerization of **OPVEx^{2}Box^{4+}** is not affected by guest molecules, thereby allowing for reversible capture and release of both π-electron-poor and π-electron-rich guests by heating and blue light irradiation, respectively. The intrinsic reason for the photocontrollable guest release may be attributed to the destruction of the preorganized (box-like) structure of the (*EE*)-**OPVEx^{2}Box^{4+}** following blue light irradiation, which results in the width of the cyclophane being broadened and its length shortened, disfavoring effective binding between host and guests. More important is the fact that the (*EZ*)-OPV^{2+} unit protrudes outside the initial plane after blue light irradiation, hindering the host and guest molecules from forming a stable sandwich-like structure.

■ CONCLUSION

A semi-rigid photo- and thermal-responsive tetracationic organic cyclophane, **OPVEx^{2}Box^{4+}**, has been shown to be interconverted reversibly between (*EE*)- and (*EZ*)-configurations by alternating blue light irradiation and heating. The reaction rate and conversion yield of the reverse isomerization were found to be significantly improved within the macrocyclic scaffold in comparison with those of non-cyclic derivatives of photoactive oligo(*p*-phenylenevinylene) bipyridinium units. The unique electronic character of the (*EE*)-isomer renders the cyclophane capable of binding both π-electron-rich and π-electron-deficient guest molecules through charge-transfer and van der Waals interactions. All the guest molecules—e.g., anthracene, perylene, **9,10-AQ** and **5,12-TQ**—can be released and bound reversibly by irradiating and heating in alternating fashion. This photo- and thermal-controlled molecular encapsulation strategy not only provides the incentive to design more-advanced photo-responsive host−guest systems and switchable molecular machines but also possesses the potential for applications in the fields of active ingredients stabilization, controllable drug release, and toxin separations.

■ ASSOCIATED CONTENT

Supporting Information

The Supporting Information is available free of charge on the ACS Publications website at DOI: 10.1021/jacs.8b10526.

Detailed synthetic procedures; crystallographic and spectroscopic (NMR, HRMS, UV−vis absorption, and fluorescence) characterization for the (*EE*)- and the (*EZ*)-isomers of **OPVEx^{2}Box**·4PF$_6$ and the complexes formed by anthracene, perylene, **9,10-AQ** and **5,12-TQ** with the (*EE*)-**OPVEx^{2}Box**·4PF$_6$, including Figures S1−S45 (PDF)

X-ray crystallographic data for (*EE*)-**OPVEx^{2}Box**·4PF$_6$ (CIF)

X-ray crystallographic data for (*EZ*)-**OPVEx^{2}Box**·4PF$_6$ (CIF)

X-ray crystallographic data for **5,12-TQ**⊂(*EE*)-**OPVEx^{2}Box**·4PF$_6$ (CIF)

X-ray crystallographic data for **9,10-AQ**⊂(*EE*)-**OPVEx^{2}Box**·4PF$_6$ (CIF)

X-ray crystallographic data for anthracene⊂(*EE*)-**OPVEx^{2}Box**·4PF$_6$ (CIF)

X-ray crystallographic data for perylene⊂(*EE*)-**OPVEx^{2}Box**·4PF$_6$ (CIF)

■ AUTHOR INFORMATION

Corresponding Authors

*yuliu@nankai.edu.cn
*stoddart@northwestern.edu

ORCID

Zhichang Liu: 0000-0003-3412-512X
Kang Cai: 0000-0002-8883-0142
Yu Liu: 0000-0001-8723-1896
J. Fraser Stoddart: 0000-0003-3161-3697

Notes

The authors declare no competing financial interest.

■ ACKNOWLEDGMENTS

This research was conducted as part of the Joint Center of Excellence in Integrated Nanosystems (JCIN) at King Abdulaziz City for Science and Technology (KACST) and Northwestern University (NU). The authors thank both KACST and NU for their continued support of this research. The authors thank the National Nature Science Foundation of China (NNSFC, Grant Nos. 21432004, 21672113, 21772099, 21861132001, and 91527301) for financial support. This work was also supported by the China Scholarship Council.

■ REFERENCES

(1) (a) Motlagh, H. N.; Wrabl, J. O.; Li, J.; Hilser, V. J. The Ensemble Nature of Allostery. *Nature* **2014**, *508*, 331−339. (b) Guo, J.; Zhou, H. X. Protein Allostery and Conformational Dynamics. *Chem. Rev.* **2016**, *116*, 6503−6515. (c) Law, A. B.; Sapienza, P. J.; Zhang, J.; Zuo, X.; Petit, C. M. Native State Volume Fluctuations in Proteins as a Mechanism for Dynamic Allostery. *J. Am. Chem. Soc.* **2017**, *139*, 3599−3602. (d) Fan, Y.; Cross, P. J.; Jameson, G. B.; Parker, E. J. Exploring Modular Allostery via Interchangeable Regulatory Domains. *Proc. Natl. Acad. Sci. U. S. A.* **2018**, *115*, 3006−3011.

(2) Riccio, A.; Vitagliano, L.; di Prisco, G.; Zagari, A.; Mazzarella, L. The Crystal Structure of a Tetrameric Hemoglobin in a Partial Hemichrome State. *Proc. Natl. Acad. Sci. U. S. A.* **2002**, *99*, 9801−9806.

(3) (a) Thordarson, P.; Bijsterveld, E. J.; Elemans, J. A.; Kasak, P.; Nolte, R. J.; Rowan, A. E. Highly Negative Homotropic Allosteric Binding of Viologens in a Double-Cavity Porphyrin. *J. Am. Chem. Soc.* **2003**, *125*, 1186−1187. (b) Mendez-Arroyo, J.; Barroso-Flores, J.; Lifschitz, A. M.; Sarjeant, A. A.; Stern, C. L.; Mirkin, C. A. A Multi-State, Allosterically-Regulated Molecular Receptor with Switchable Selectivity. *J. Am. Chem. Soc.* **2014**, *136*, 10340−10348. (c) Mendez-Arroyo, J.; d'Aquino, A. I.; Chinen, A. B.; Manraj, Y. D.; Mirkin, C. A. Reversible and Selective Encapsulation of Dextromethorphan and β-Estradiol Using an Asymmetric Molecular Capsule Assembled via the Weak-Link Approach. *J. Am. Chem. Soc.* **2017**, *139*, 1368−1371.

(4) (a) Pedersen, C. J. Cyclic Polyethers and Their Complexes with Metal Salts. *J. Am. Chem. Soc.* **1967**, *89*, 2495−2496; **1967**, *89*, 7017−7036. (b) Bright, D.; Truter, M. R. Crystal Structure of a Cyclic Polyether Complex of Alkali Metal Thiocyanate. *Nature* **1970**, *225*,

176–177. (c) Pedersen, C. J. Crystalline Salt Complexes of Macrocyclic Polyethers. *J. Am. Chem. Soc.* **1970**, *92*, 386–391. (d) Cram, D. J. The Design of Molecular Hosts, Guests, and Their Complexes (Nobel Lecture). *Angew. Chem., Int. Ed. Engl.* **1988**, *27*, 1009–1020. (e) Lehn, J.-M. Supramolecular Chemistry—Scope and Perspectives Molecules, Supermolecules, and Molecular Devices (Nobel Lecture). *Angew. Chem., Int. Ed. Engl.* **1988**, *27*, 89–112.

(5) (a) Alston, D. R.; Slawin, A. M. Z.; Stoddart, J. F.; Williams, D. J.; Zarzycki, R. Second Sphere Coordination Adducts of Phosphane-Transition Metal Complexes with β-Cyclodextrin and its Methylated Derivative. *Angew. Chem., Int. Ed. Engl.* **1988**, *27*, 1184–1185. (b) Harada, A.; Li, J.; Kamachi, M. The Molecular Necklace: A Rotaxane Containing Many Threaded α-Cyclodextrins. *Nature* **1992**, *356*, 325–327. (c) Wenz, G. Cyclodextrins as Building-Blocks for Supramolecular Structures and Functional Units. *Angew. Chem., Int. Ed. Engl.* **1994**, *33*, 803–822. (d) Liu, Y.; Ke, C. F.; Zhang, H. Y.; Cui, J.; Ding, F. Complexation-Induced Transition of Nanorod to Network Aggregates: Alternate Porphyrin and Cyclodextrin Arrays. *J. Am. Chem. Soc.* **2008**, *130*, 600–605. (e) Tafazzoli, M.; Ghiasi, M. Structure and Conformation of α-, β- and γ-Cyclodextrin in Solution: Theoretical Approaches and Experimental Validation. *Carbohydr. Polym.* **2009**, *78*, 10–15.

(6) (a) Gutsche, C. D.; Dhawan, B.; No, K. H.; Muthukrishnan, R. Calixarenes. 4. The Synthesis, Characterization, and Properties of the Calixarenes from *p-tert*-Butylphenol. *J. Am. Chem. Soc.* **1981**, *103*, 3782–3792. (b) Gutsche, C. D.; Bauer, L. J. Calixarenes. 13. The Conformational Properties of Calix[4]arenes, Calix[6]arenes, Calix[8]arenes, and Oxacalixarenes. *J. Am. Chem. Soc.* **1985**, *107*, 6052–6059. (c) Shinkai, S. Calixarenes—The Third Generation of Supramolecules. *Tetrahedron* **1993**, *49*, 8933–8968. (d) Ikeda, A.; Shinkai, S. Novel Cavity Design Using Calix[n]arene Skeletons: Toward Molecular Recognition and Metal Binding. *Chem. Rev.* **1997**, *97*, 1713–1734. (e) Hanna, T. A.; Liu, L.; Angeles-Boza, A. M.; Kou, X.; Gutsche, C. D.; Ejsmont, K.; Watson, W. H.; Zakharov, L. N.; Incarvito, C. D.; Rheingold, A. L. Synthesis, Structures, and Conformational Characteristics of Calixarene Monoanions and Dianions. *J. Am. Chem. Soc.* **2003**, *125*, 6228–6238.

(7) (a) Ogoshi, T.; Kanai, S.; Fujinami, S.; Yamagishi, T. A.; Nakamoto, Y. *para*-Bridged Symmetrical Pillar[5]arenes: Their Lewis Acid Catalyzed Synthesis and Host–Guest Property. *J. Am. Chem. Soc.* **2008**, *130*, 5022–5023. (b) Cragg, P. J.; Sharma, K. Pillar[5]arenes: Fascinating Cyclophanes with a Bright Future. *Chem. Soc. Rev.* **2012**, *41*, 597–607. (c) Xue, M.; Yang, Y.; Chi, X.; Zhang, Z.; Huang, F. Pillararenes, A New Class of Macrocycles for Supramolecular Chemistry. *Acc. Chem. Res.* **2012**, *45*, 1294–1308. (d) Li, S. H.; Zhang, H. Y.; Xu, X.; Liu, Y. Mechanically Selflocked Chiral Gemini-Catenanes. *Nat. Commun.* **2015**, *6*, 7590.

(8) (a) Sugasaki, A.; Ikeda, M.; Takeuchi, M.; Koumoto, K.; Shinkai, S. The First Example of Positive Allosterism in an Aqueous Saccharide-Binding System Designed on a Ce(IV) Bis(porphyrinate) Double Decker Scaffold. *Tetrahedron* **2000**, *56*, 4717–4723. (b) Perlmutter-Hayman, B. Cooperative Binding to Macromolecules. A Formal Approach. *Acc. Chem. Res.* **1986**, *19*, 90–96.

(9) Chen, S.; Yamasaki, M.; Polen, S.; Gallucci, J.; Hadad, C. M.; Badjić, J. D. Dual-Cavity Basket Promotes Encapsulation in Water in an Allosteric Fashion. *J. Am. Chem. Soc.* **2015**, *137*, 12276–12281.

(10) Gianneschi, N. C.; Bertin, P. A.; Nguyen, S. T.; Mirkin, C. A.; Zakharov, L. N.; Rheingold, A. L. A Supramolecular Approach to an Allosteric Catalyst. *J. Am. Chem. Soc.* **2003**, *125*, 10508–10509.

(11) Ghale, G.; Nau, W. M. Dynamically Analyte-Responsive Macrocyclic Host-Fluorophore Systems. *Acc. Chem. Res.* **2014**, *47*, 2150–2159.

(12) (a) Barnes, J. C.; Juriček, M.; Strutt, N. L.; Frasconi, M.; Sampath, S.; Giesener, M. A.; McGrier, P. L.; Bruns, C. J.; Stern, C. L.; Sarjeant, A. A.; Stoddart, J. F. ExBox: A Polycyclic Aromatic Hydrocarbon Scavenger. *J. Am. Chem. Soc.* **2013**, *135*, 183–192. (b) Wu, G.; Wang, C. Y.; Jiao, T.; Zhu, H.; Huang, F.; Li, H. Controllable Self-Assembly of Macrocycles in Water for Isolating Aromatic Hydrocarbon Isomers. *J. Am. Chem. Soc.* **2018**, *140*, 5955–5961. (c) Jie, K.; Liu, M.; Zhou, Y.; Little, M. A.; Pulido, A.; Chong, S. Y.; Stephenson, A.; Hughes, A. R.; Sakakibara, F.; Ogoshi, T.; Blanc, F.; Day, G. M.; Huang, F.; Cooper, A. I. Near-Ideal Xylene Selectivity in Adaptive Molecular Pillar[*n*]arene Crystals. *J. Am. Chem. Soc.* **2018**, *140*, 6921–6930.

(13) (a) Ryan, S. T.; Del Barrio, J.; Suardiaz, R.; Ryan, D. F.; Rosta, E.; Scherman, O. A. A Dynamic and Responsive Host in Action: Light-Controlled Molecular Encapsulation. *Angew. Chem., Int. Ed.* **2016**, *55*, 16096–16100. (b) Kurihara, K.; Yazaki, K.; Akita, M.; Yoshizawa, M. A Switchable Open/Closed Polyaromatic Macrocycle that Shows Reversible Binding of Long Hydrophilic Molecules. *Angew. Chem., Int. Ed.* **2017**, *56*, 11360–11364. (c) Ke, X. S.; Kim, T.; Brewster, J. T., II; Lynch, V. M.; Kim, D.; Sessler, J. L. Expanded Rosarin: A Versatile Fullerene (C60) Receptor. *J. Am. Chem. Soc.* **2017**, *139*, 4627–4630. (d) Tang, J. H.; Sun, Y.; Gong, Z. L.; Li, Z. Y.; Zhou, Z.; Wang, H.; Li, X.; Saha, M. L.; Zhong, Y. W.; Stang, P. J. Temperature-Responsive Fluorescent Organoplatinum(II) Metallacycles. *J. Am. Chem. Soc.* **2018**, *140*, 7723–7729.

(14) (a) Szaloki, G.; Croue, V.; Carre, V.; Aubriet, F.; Aleveque, O.; Levillain, E.; Allain, M.; Arago, J.; Orti, E.; Goeb, S.; Salle, M. Controlling the Host–Guest Interaction Mode through a Redox Stimulus. *Angew. Chem., Int. Ed.* **2017**, *56*, 16272–16276. (b) Black, S. P.; Stefankiewicz, A. R.; Smulders, M. M.; Sattler, D.; Schalley, C. A.; Nitschke, J. R.; Sanders, J. K. Generation of a Dynamic System of Three-Dimensional Tetrahedral Polycatenanes. *Angew. Chem., Int. Ed.* **2013**, *52*, 5749–5752.

(15) (a) Wu, Z. Q.; Shao, X. B.; Li, C.; Hou, J. L.; Wang, K.; Jiang, X. K.; Li, Z. T. Hydrogen-Bonding-Driven Preorganized Zinc Porphyrin Receptors for Efficient Complexation of C_{60}, C_{70}, and C_{60} Derivatives. *J. Am. Chem. Soc.* **2005**, *127*, 17460–17468. (b) Degen, P.; Leick, S.; Rehage, H.; Polkowska, J.; Klarner, F. G. Gemini-Like Molecular Clips and Tweezers: The Influence of Structure and Guest Binding on Interfacial Tension. *Langmuir* **2009**, *25*, 6094–6099.

(16) (a) Murase, T.; Sato, S.; Fujita, M. Switching the Interior Hydrophobicity of a Self-Assembled Spherical Complex through the Photoisomerization of Confined Azobenzene Chromophores. *Angew. Chem., Int. Ed.* **2007**, *46*, 5133–5136. (b) Han, M.; Michel, R.; He, B.; Chen, Y. S.; Stalke, D.; John, M.; Clever, G. H. Light-Triggered Guest Uptake and Release by a Photochromic Coordination Cage. *Angew. Chem., Int. Ed.* **2013**, *52*, 1319–1323. (c) Border, S. E.; Pavlović, R. Z.; Zhiquan, L.; Badjić, J. D. Removal of Nerve Agent Simulants from Water Using Light-Responsive Molecular Baskets. *J. Am. Chem. Soc.* **2017**, *139*, 18496–18499.

(17) (a) Wu, H.; Chen, Y.; Liu, Y. Reversibly Photoswitchable Supramolecular Assembly and Its Application as a Photoerasable Fluorescent Ink. *Adv. Mater.* **2017**, *29*, 1605271. (b) Lubbe, A. S.; Szymanski, W.; Feringa, B. L. Recent Developments in Reversible Photoregulation of Oligonucleotide Structure and Function. *Chem. Soc. Rev.* **2017**, *46*, 1052–1079. (c) Qian, H.; Wang, Y. Y.; Guo, D. S.; Aprahamian, I. Controlling the Isomerization Rate of an Azo-BF_2 Switch Using Aggregation. *J. Am. Chem. Soc.* **2017**, *139*, 1037–1040. (d) Park, K. M.; Baek, K.; Ko, Y. H.; Shrinidhi, A.; Murray, J.; Jang, W. H.; Kim, K. H.; Lee, J. S.; Yoo, J.; Kim, S.; Kim, K. Mono-Allyloxylated Cucurbit[7]uril Acts as an Unconventional Amphiphile to Form Light-Responsive Vesicles. *Angew. Chem., Int. Ed.* **2018**, *57*, 3132–3136.

(18) Qu, D. H.; Wang, Q. C.; Zhang, Q. W.; Ma, X.; Tian, H. Photoresponsive Host–Guest Functional Systems. *Chem. Rev.* **2015**, *115*, 7543–7588.

(19) Reuter, R.; Wegner, H. A. Oligoazobenzenophanes—Synthesis, Photochemistry and Properties. *Chem. Commun.* **2011**, *47*, 12267–12276.

(20) Odell, B.; Reddington, M. V.; Slawin, A. M. Z.; Spencer, N.; Stoddart, J. F.; Williams, D. J. Cyclobis(paraquat-*p*-phenylene). A Tetracationic Multipurpose Receptor. *Angew. Chem., Int. Ed. Engl.* **1988**, *27*, 1547–1550.

(21) Ashton, P. R.; Brown, C. L.; Chrystal, E. J. T.; Goodnow, T. T.; Kaifer, A. E.; Parry, K. P.; Philp, D.; Slawin, A. M. Z.; Spencer, N.;

Stoddart, J. F.; Williams, D. J. The Self-Assembly of a Highly Ordered [2]Catenane. *J. Chem. Soc., Chem. Commun.* **1991**, 634−639.

(22) Philp, D.; Slawin, A. M. Z.; Spencer, N.; Stoddart, J. F.; Williams, J. D. The Complexation of Tetrathiafulvalene by Cyclobis-(paraquat-*p*-phenylene). *J. Chem. Soc., Chem. Commun.* **1991**, 1584−1586.

(23) Stoddart, J. F. The Chemistry of the Mechanical Bond. *Chem. Soc. Rev.* **2009**, *38*, 1802−1820.

(24) Juríček, M.; Barnes, J. C.; Dale, E. J.; Liu, W. G.; Strutt, N. L.; Bruns, C. J.; Vermeulen, N. A.; Ghooray, K. C.; Sarjeant, A. A.; Stern, C. L.; Botros, Y. Y.; Goddard, W. A., III; Stoddart, J. F. Ex^{2}Box: Interdependent Modes of Binding in a Two-Nanometer-Long Synthetic Receptor. *J. Am. Chem. Soc.* **2013**, *135*, 12736−12746.

(25) Gong, X.; Young, R. M.; Hartlieb, K. J.; Miller, C.; Wu, Y.; Xiao, H.; Li, P.; Hafezi, N.; Zhou, J.; Ma, L.; Cheng, T.; Goddard, W. A., III; Farha, O. K.; Hupp, J. T.; Wasielewski, M. R.; Stoddart, J. F. Intramolecular Energy and Electron Transfer within a Diazaperopyrenium-Based Cyclophane. *J. Am. Chem. Soc.* **2017**, *139*, 4107−4116.

(26) (a) Juskowiak, B.; Takenaka, S.; Takagi, M. DNA-Controlled Photoisomerization of Bis(2-(1-methyl-pyridinium-4-yl)vinyl)-benzene. *Chem. Lett.* **1999**, *28*, 209−210. (b) Zhu, L.; Ang, C. Y.; Li, X.; Nguyen, K. T.; Tan, S. Y.; Agren, H.; Zhao, Y. Luminescent Color Conversion on Cyanostilbene-Functionalized Quantum Dots via In-situ Photo-Tuning. *Adv. Mater.* **2012**, *24*, 4020−4024. (c) Zhu, L.; Li, X.; Zhang, Q.; Ma, X.; Li, M.; Zhang, H.; Luo, Z.; Agren, H.; Zhao, Y. Unimolecular Photoconversion of Multicolor Luminescence on Hierarchical Self-Assemblies. *J. Am. Chem. Soc.* **2013**, *135*, 5175−5182. (d) Yan, X.; Xu, J. F.; Cook, T. R.; Huang, F.; Yang, Q. Z.; Tung, C. H.; Stang, P. J. Photoinduced Transformations of Stiff-Stilbene-Based Discrete Metallacycles to Metallosupramolecular Polymers. *Proc. Natl. Acad. Sci. U. S. A.* **2014**, *111*, 8717−8722. (e) Mandal, A. K.; Sreejith, S.; He, T.; Maji, S. K.; Wang, X. J.; Ong, S. L.; Joseph, J.; Sun, H.; Zhao, Y. Three-Photon-Excited Luminescence from Unsymmetrical Cyanostilbene Aggregates: Morphology Tuning and Targeted Bioimaging. *ACS Nano* **2015**, *9*, 4796−4805.

(27) Wei, P.; Zhang, J. X.; Zhao, Z.; Chen, Y.; He, X.; Chen, M.; Gong, J.; Sung, H. H.; Williams, I. D.; Lam, J. W. Y.; Tang, B. Z. Multiple yet Controllable Photoswitching in a Single AIEgen System. *J. Am. Chem. Soc.* **2018**, *140*, 1966−1975.

(28) Dale, E. J.; Vermeulen, N. A.; Juríček, M.; Barnes, J. C.; Young, R. M.; Wasielewski, M. R.; Stoddart, J. F. Supramolecular Explorations: Exhibiting the Extent of Extended Cationic Cyclophanes. *Acc. Chem. Res.* **2016**, *49*, 262−273.

(29) Dale, E. J.; Vermeulen, N. A.; Thomas, A. A.; Barnes, J. C.; Juríček, M.; Blackburn, A. K.; Strutt, N. L.; Sarjeant, A. A.; Stern, C. L.; Denmark, S. E.; Stoddart, J. F. *J. Am. Chem. Soc.* **2014**, *136*, 10669−10682.

DOI: 10.1021/jacs.8b10526